Retinotopic Mapping of the Human Visual Cortex Using a Compact High-Density DOT System

Chandran V. Seshagiri[1], Tanmayi Oruganti[1], Jason W. Trobaugh[1,2], Joseph P. Culver[3], Bertan Hallacoglu[1]

(1) Cephalogics, LLC, Boston, MA 02110
(2) Department of Electrical and Systems Engineering, Washington University in St. Louis, St. Louis, MO 63110
(3) Department of Radiology, Washington University in St. Louis, St. Louis, MO 63110

Organization for Human Brain Mapping

Outline

With large arrays of spatially distributed near-infrared sources and photodetectors, Diffuse Optical Tomography (DOT) systems have been used to image the spatially varying distribution of the concentrations of chromophores such as oxy- and deoxy-hemoglobin. Traditional DOT systems rely on fiber optic cables to carry optical signals to and from the imaged tissue. As the number of channels increases, the weight and size of the optical fibers limit both the comfort and practical utility of such systems in clinical use.

We have developed a compact, multi-channel and multi-wavelength continuous wave DOT imaging system that does not use fiber optic cables. To validate the performance of our system *in vivo*, we performed retinotopic mapping of the visual cortex as previously described by fMRI studies [1] and other HD-DOT systems [2,3].

The results presented here replicate earlier work with a fiber-based HD-DOT system [3] and demonstrate that similar spatial mapping of the human visual cortex is achievable in a compact, easy-to-use HD-DOT device.

Hardware System

DOT System

- High-density arrangement: 10x18 (sources x detectors) on rigid-flex circuit boards (Fig. 1a).
- Five time-encoded, amplitude-modulated VCSELs operate at five wavelengths ranging from 688-850nm within each source optode.
- Silicon Photodiodes with 7.0 mm^2 detection area
- Detected signals demodulated via a synchronous detection demodulation scheme
- Source-detector distances range from 13-87mm
- 180 channels per wavelength collected at 5Hz frame-rate. Acquired data is digitized, processed, and transmitted to a laptop via Ethernet connection for post-processing (fiber-free interface)
- Dynamic range of over 140 dB (NEP $\approx 0.14\text{pW}/\sqrt{hz}$)

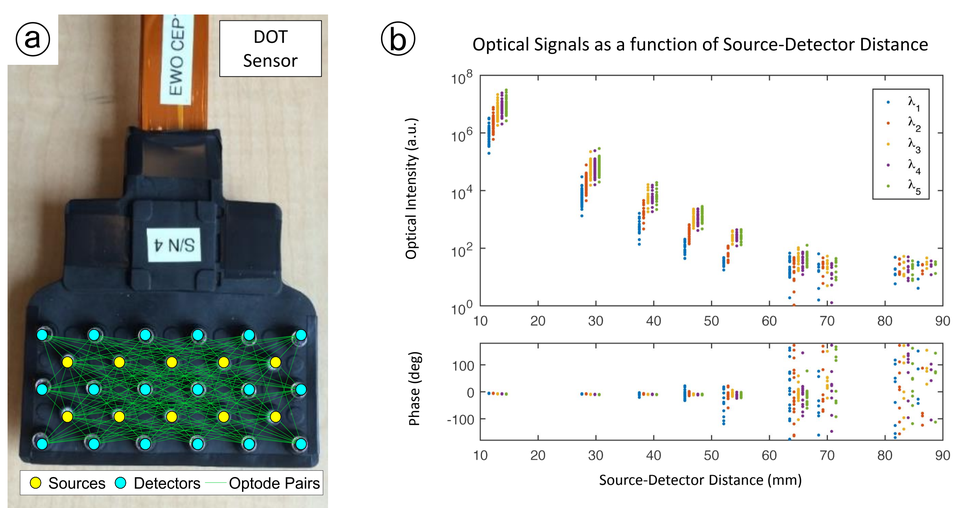

Figure 1: DOT Sensor array and example data from a human subject. (a) Photo of the high density prototype DOT sensor array containing 10 sources (yellow) and 18 detectors (blue). Green lines show all measurement pairs ranging from 13-87mm. (b) Example optical signal intensities and phase as a function of source-detector distance

Methods

Retinotopy Experimental Protocol

- Two healthy subjects enrolled and provided informed consent (WIRB Study # 1132591)
- Subjects were seated approximately 30 inches from a computer screen; the screen was height adjusted for each subject
- A sensor was applied to the back of each subject's head just above the inion to maximize coverage of the primary visual cortex
- Rotating Checkerboard Wedge Stimulus
  - 60^o wedge width with alternating (10Hz) checkboard pattern
  - Wedges rotate at 10^0 steps/sec (one full rotation = 36s)

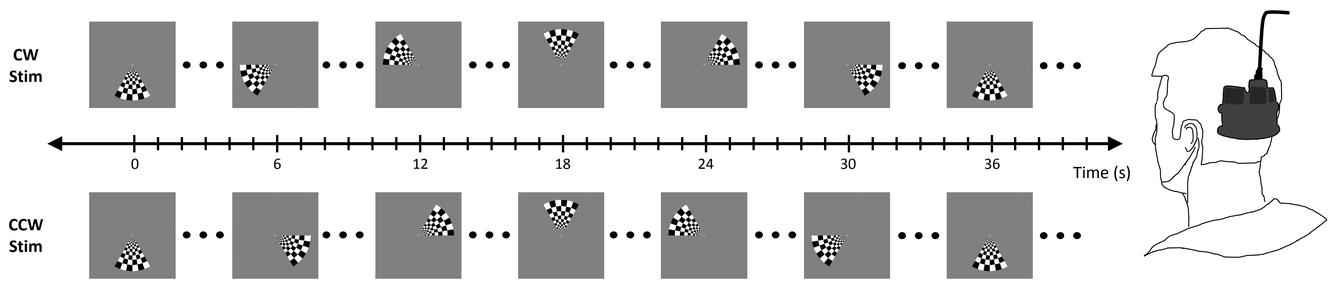

- 10 full revolutions of the wedge stimulus presented with rotation either *clockwise* (**CW**) or *counterclockwise* (**CCW**)
- Subjects were instructed to maintain focus on the crosshairs at the center of the monitor at all times
- Subjects were seated in a dark room and wore passive noise canceling headphones to minimize distraction

Data Processing and HbO & HbR reconstruction

- Data from all optode pairs bandpass filtered (0.02Hz-0.5Hz) and downsampled to 1Hz, giving one sample per stimulus wedge position
- Signals with low SNR were removed from the analysis
- Rytov approximation, expressed as $y = -\log(\phi/\phi_0) = Ax$, was used for estimation of voxelized HbO and HbR perturbations, where:
  - ϕ is the measured light intensities (*e.g.* Fig. 1b) at any given time point
  - ϕ_0 is the mean of the signals across all ten stimulus presentations
  - x is a vector of the changes in HbO and HbR for all voxels in the imaging volume
  - A is the chromophore sensitivity matrix for the specific sensor-array geometry constructed according to [3]. Finite-element modeling in a two-layered slab model was performed using NIRFAST to generate Green's functions for the sensitivities of each source and detector for all wavelengths [4]
- Moore-Penrose generalized inverse [3] was used for the estimation of HbO and HbR perturbation images, $x = A^{\#}y$, by minimizing the objective function: $\min\{\|(y - Ax)\|_2^2 + \alpha\|Lx\|_2^2\}$, where $A^{\#} = L^{-1}A^T(A^TA + \alpha I)^{-1}$, $L = \sqrt{diag(A^TA) + \beta}$, and α and β represent regularization values [3]
- Measurements were processed into 2-D images of the brain layer with 2mm pixel size

Polar Angle Mapping

- The cross-correlation between ΔHbO temporal trends and a sinusoid with period = 36s was computed for every voxel as illustrated in Figure 2
- The max amplitude of the cross-correlation for each voxels was used to assess the strength of the periodicity
- The lag of the max amplitude was mapped to the polar angle of the rotating wedge stimulus at the time of the lag [including a delay to account for the neurovascular coupling delay]
- A constant contour at 10% of the max correlation strength is shown to denote the region where we have the highest sensitivity and strongest response

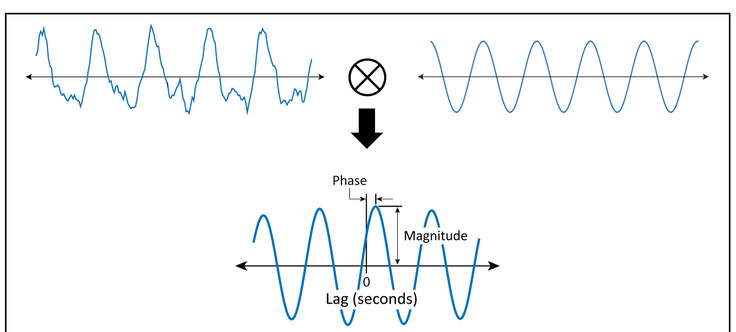

Figure 2: Example of mapping polar angle from the ΔHbO temporal trend. Phase lag and magnitude of cross-correlation with sinusoid (period = 36s) are used to measure polar angle and strength of correlation.

Results

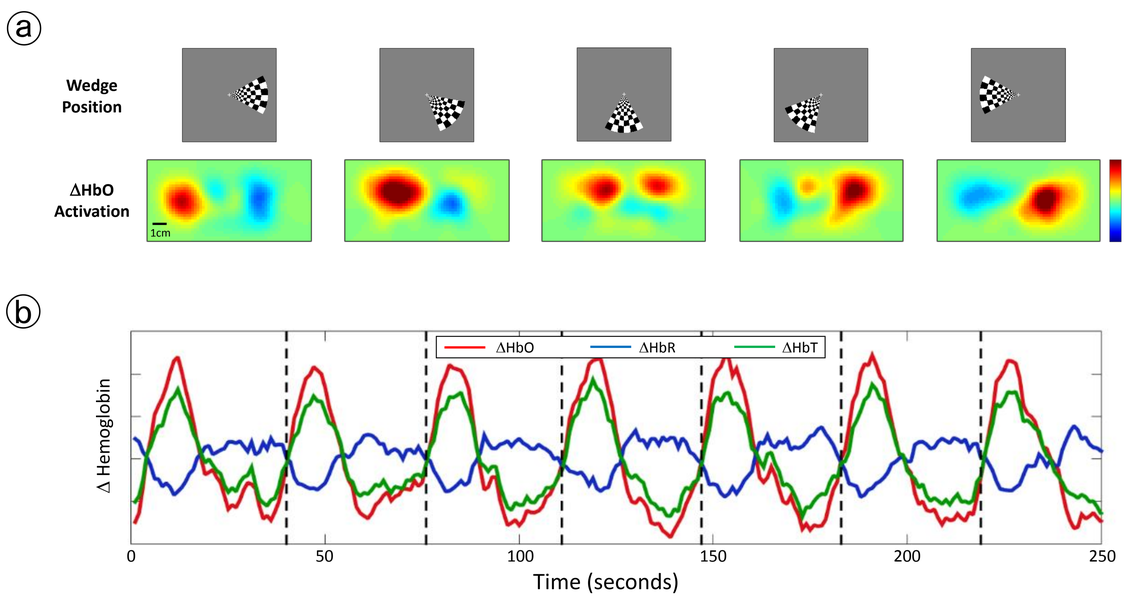

Figure 3: Activation images and hemoglobin temporal trends. (a) ΔHbO activation images for five different wedge positions. As expected, activation is mapped to visual cortex positions contralateral and inverted to the presented wedge position. (b) Temporal trends of ΔHbO (red), ΔHbR (blue), and ΔHbT (green) from a randomly selected pixel in the imaging field. Trend covers 7 cycles of the rotating wedge (dashed lines indicate the start of each revolution). The trends show the strong periodic nature of the ΔHbO activation

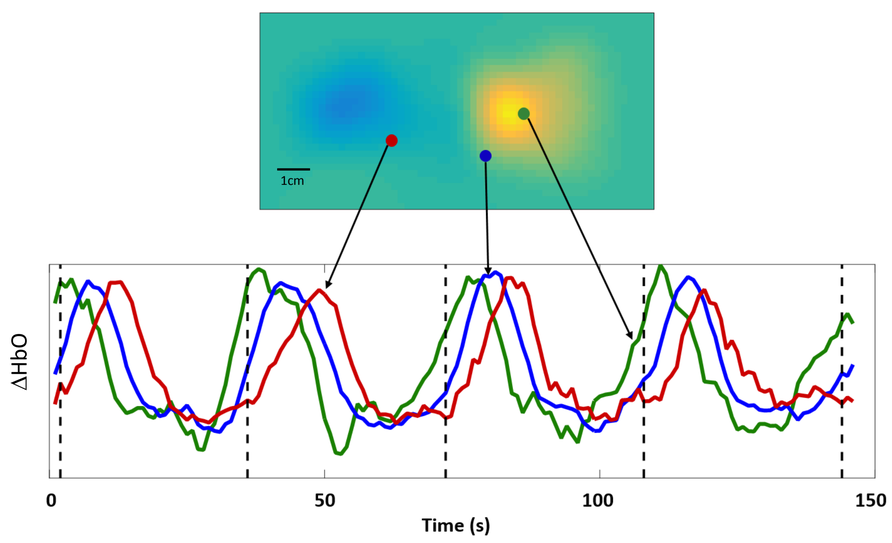

Figure 4: Temporal trends of ΔHbO for four cycles of the rotating wedge shown for three different spatial positions in the imaging field. All three locations are strongly periodic with the stimulus presentation, but each location is maximally stimulated at different times. The times correspond to the wedge position that the cortical tissue is maximally sensitive to at each location

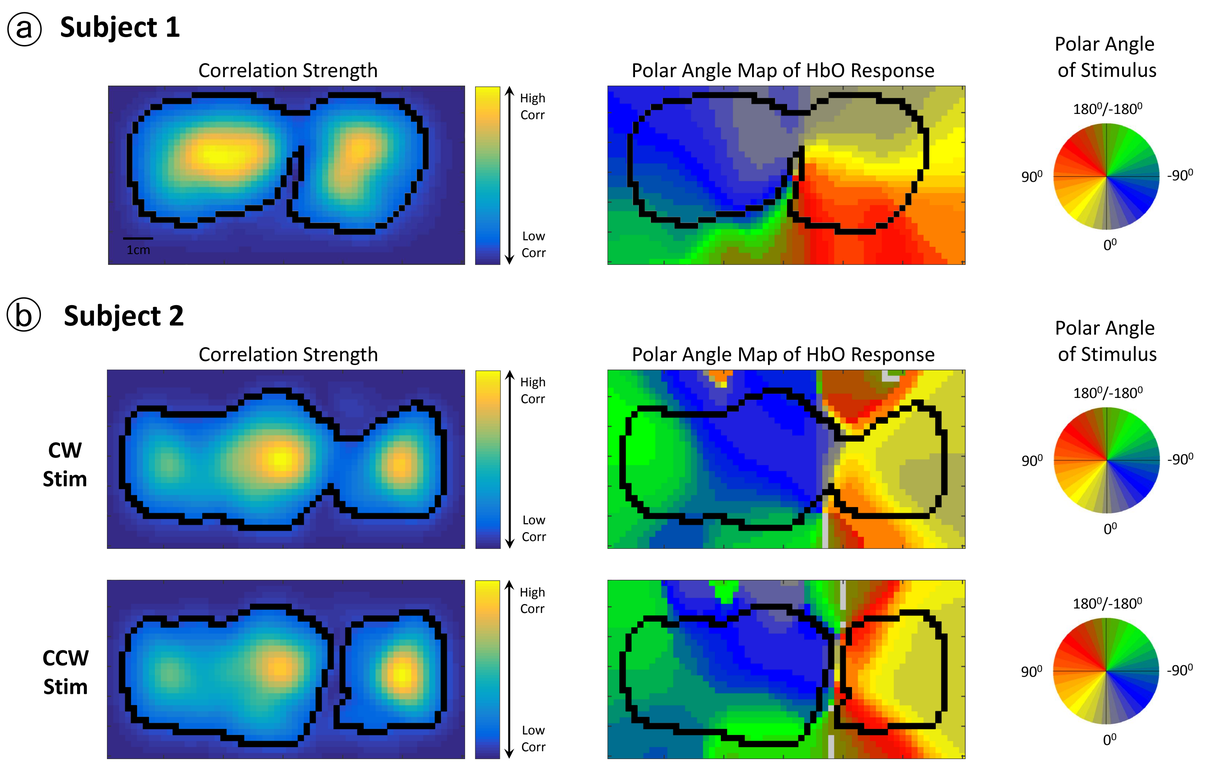

Figure 5: Polar Angle mapping in Subjects 1 and 2. (a) Polar Angle Map and Correlation Strength for Subject 1. The Correlation Strength plot highlights the strong activation of the two hemispheres. The black outline indicates the 90% contour of the correlation strength. The polar angle map of the HbO response shows the mapping of polar angle across the entire imaging field with a mask based on the 90% contour of the correlation strength. (b) Results for both clockwise and counterclockwise stimulation in subject 2. While the polar angle map is slightly different from subject 1, the repeatability for the CW and CCW stimuli highlights the repeatability of the results within this subject

Discussion and Conclusions

- We have demonstrated that our new, compact, non fiber-optic HD-DOT system is capable of generating detailed maps of the activation of primary visual cortex to stimuli that vary across the spatial visual field
- Results from both subjects show many spatial similarities with each quadrant of the visual field well mapped to similar regions of the visual cortex. Differences between the two subjects may reflect differences in the folding of the cortical surfaces
- The extreme similarities in the spatial map with clockwise and counter-clockwise stimulation of Subject 2 show repeatability of the spatial mapping within a subject
- These results demonstrate that our compact, wearable HD-DOT system is capable of replicating cortical stimulus mapping studies that have previously required larger fiber-based DOT systems or functional MRI imaging

References

[1] S.A. Engel, G.H. Glover, B.A. Wandell, (1997) **Cerebral Cortex**, 7: 181-192
[2] G.R. Wylie, H.L. Graber, G.T. Voelbel, A.D. Kohl, J DeLuca, Y. Pei, Y. Xu, R.L. Barbour, (2009) **NeuroImage**, 47: 473-481
[3] B. W. Zeff, B. R. White, H. Dehghani, B. L. Schlaggar, J. P. Culver, (2007) **PNAS**, 104: 12169-12174.
[4] H. Dehghani, M. E. Eames, P. K. Yalavarthy, S. C. Davis, S. Srinivasan, C. M. Carpenter, B. W. Pogue, and K. D. Paulsen, **Commun. Numer. Methods Eng.** (2009) 25: 711–732.